Journal of
Nanoscience and Nanotechnology
Vol. 15, 1–9, 2015
www.aspbs.com/jnn

Sesamum indicum Plant Extracted Microwave Combustion Synthesis and Opto-Magnetic Properties of Spinel $Mn_xCo_{1-x}Al_2O_4$ Nano-Catalysts

A. Manikandan[1,*], M. Durka[2], M. Amutha Selvi[3], and S. Arul Antony[1,*]

[1] *PG and Research Department of Chemistry, Presidency College (Autonomous), Chennai 600005, India*
[2] *Department of Physics, A. V. V. M Sri Pushpam College (Autonomous), Poondi, Thanjavur 613503, Tamil Nadu, India*
[3] *Department of Chemistry, Avinashilingam Institute for Home Science and Higher Education for Women University, Coimbatore 641043, India*

Spinel $Mn_xCo_{1-x}Al_2O_4$ ($x = 0$, 0.3 and 0.5) nanoparticles were synthesized using *Sesamum indicum (S. indicum)* plant extracted microwave-assisted combustion method. *S. indicum* plant extract simplifies the process, provides an alternative process for a simple, economical and environment friendly synthesis. The absence of surfactant/catalysts has led to a simple, cheap and fast method of synthesis of spinel nanoparticles. The as-synthesized spinel nanoparticles were characterized by X-ray diffraction (XRD), Fourier transform infrared (FT-IR) spectroscopy, high resolution scanning electron microscopy (HR-SEM), high resolution transmission electron microscopy (HR-TEM), energy dispersive X-ray analysis (EDX), Brunauer Emmett Teller (BET) surface area analysis, UV-Visible diffuse reflectance spectroscopy (DRS), Photoluminescence (PL) spectroscopy, and vibrating sample magnetometer. The formation of spinel nanoparticles was confirmed by HR-SEM and HR-TEM and their possible formation mechanisms were also proposed. Powder XRD, FT-IR, SAED and EDX results confirmed the formation of pure and single cubic phase $CoAl_2O_4$ with well-defined crystalline. The optical property was determined by DRS and PL spectra. VSM measurements revealed that pure and Mn-doped $CoAl_2O_4$ samples have weak ferromagnetic behavior and the magnetization values increases with increasing the concentration of Mn^{2+} ions in the $CoAl_2O_4$ lattice. Sample $Mn_{0.5}Co_{0.5}Al_2O_4$ possesses a higher surface area, smaller crystallite size than other samples, which led to enhance the performance toward the selective oxidation of benzyl alcohol into benzaldehyde.

Keywords: Spinel, Nanoparticles, Cobalt Aluminate, *Sesamum indicum* Extract, Opto-Magnetic Properties, Catalytic Properties.

1. INTRODUCTION

Recently, nanostructured materials signify an attractive in nanoscience and nanotechnology, due to novel physical, electrical, optical, magnetic and catalytic property than that of bulk materials.[1–10] Spinel nanocrystalline materials are classes of binary transition metal oxides signify an attractive in the past decade, due to their small size exhibits novel physical and chemical properties leads to a various potential applications.[11,12] Among various transition metal oxides, spinel cobalt aluminate ($CoAl_2O_4$), has gained lot of attention in multidisciplinary areas, due to their efficiency in ceramics, electronic, optical, catalyst, catalyst supports, aerospace, paints, dielectrics and sensing applications.[13–16] Spinel $CoAl_2O_4$ offers many favorable properties such as mechanical strength, thermal stability, and low temperature sintering ability, high chemical stability, wide band-gap energy, excellent optical transparency and good metal dispersion capacity.[17,18] Spinel $CoAl_2O_4$ is largely used in paints for coloration, ceramics, enamels, paper, plastics, rubber and fibers.[19]

A variety of methods have been used for the preparation of spinel $CoAl_2O_4$ nanostructures such as low-temperature, such as sol–gel, hydrolysis, and polymerized complex methods.[20–23] However, the above conventional methods desirable costly equipments, materials and laborious synthetic procedures, thus leading to the tedious polluting

*Authors to whom correspondence should be addressed.

process. Recently, a novel and facile method has been used to prepare nanomaterials with high surface area, called microwave-assisted combustion method (MACM). In this MACM approach the samples are prepared at low temperatures, low cost with good control of size, structure and morphology, due to its fast reaction kinetics, cleanliness and efficiency.[24, 25] Also, MACM route of preparation is easy, fast and low energy with soft method than the above said methods.[26–28] Furthermore, to our knowledge, no literature is available on the synthesis, structural, opto-magnetic and catalytic properties of Mn-doped $CoAl_2O_4$ nanostructures by a simple MACM route.

Moreover, simple and cost effective methods to synthesize $CoAl_2O_4$ nanostructures by cheap, nontoxic and environmentally benign precursors are still the key issues. Therefore, the present study was the synthesis of pure and Mn-doped $CoAl_2O_4$ nanostructures by using green method on extract from *Sesamum indicum (S. indicum)* and determines the potential catalytic oxidation of benzyl alcohol into benzaldehyde. *Sesame* plant belongs to the family *Pedaliaceae* and genus *Sesamum*. The genus consists of about 36 species of which 19 species are indigenous to Africa.[29] To our knowledge, no literature is available on the synthesis and opto-magnetic and catalytic properties of pure and Mn-doped $CoAl_2O_4$ nanostructures by a simple *S. indicum* plant extracted MACM route. However, in our present case, the samples were prepared using *S. indicum* plant extracted MACM is a green synthesis non-polluting with low cost. Spinel $CoAl_2O_4$ nanostructures have been used extensively as a heterogeneous catalyst and it can be recovered easily from the reaction mixture by simple filtration and reused several times. Moreover, spinel $CoAl_2O_4$ is non-toxic, inexpensive, relatively high surface areas and these properties make them suitable for use as economically and environmentally viable solid heterogeneous catalysts. Generally, two main factors affecting the catalytic property of catalysts are the specific surface area and particle size, and typically a high surface area goes along with small particle size, which enhances the catalytic activity. The as-prepared samples were characterized by powder XRD, FT-IR, HR-SEM, HR-TEM, EDX, DRS, PL spectra and VSM techniques and the obtained results are discussed. The product formed by the catalytic oxidation of benzyl alcohol into benzaldehyde was characterized by gas chromatography (GC). Catalytic activity tests of benzyl alcohol were carried out and reported the influence of Mn^{2+}-dopant on catalytic activity of spinel $CoAl_2O_4$ nanocatalysts. The best activity and selectivity towards catalytic oxidation of benzyl alcohol were observed.

2. EXPERIMENTAL PART

2.1. Materials and Methods

All the chemicals used in this study were of analytical grade obtained from Merck, India and were used as received without further purification. All chemicals such as nitrates of cobalt, manganese and aluminium, and *Sesamum indicum* plant extract as the reducing agent were used for this method. The *Sesamum indicum* leaves were collected from the local agricultural fields, Athanur, Peravurani, Thanjavur 614804, Tamil Nadu, India. *S. indicum* plant extracted solution was prepared from a 5 g portion of thoroughly washed *S. indicum* leaves were finely cut and the gel obtained was dissolved in 10 ml of de-ionized water and stirred for 30 min to obtain a clear solution. The resulting product was used as an *S. indicum* plant extracted solution.

In the preparation of $CoAl_2O_4$ samples, aluminium nitrate (10 mmol) and cobalt nitrate (5 mmol) were first dissolved in the *S. indicum* plant extracted solution under vigorous stirring at room temperature for 1 h until a clear transparent solution was obtained. In this preparation process, *S. indicum* plant extracted solution has a double function of both reducing and gelling agent for the synthesis of mixed metal oxides. Metal nitrate salts and the *S. indicum* plant extracted solution were chosen by considering the total reducing and oxidizing agent valences of the raw materials and were quantified in equivalence of NOx reduction (N_2O to N_2, CO_2 and H_2O) at a low temperature. The precursor mixture of metal nitrates in *S. indicum* extracted solution was placed in a domestic microwave oven and exposed to the microwave energy in a 2.45 GHz multimode cavity at 850 W for 10 minutes (Scheme 1). Initially, the precursor mixture boiled and underwent evaporation followed by the decomposition with the evolution of gases. When the solution reached the point of spontaneous combustion, it vaporized and instantly became a solid. After completion of the reaction, the obtained solid powder was then washed with ethanol and dried at 70 °C for 1 h. The samples were prepared with the addition of Mn^{2+} of different molar ratios ($Mn_xCo_{1-x}Al_2O_4$: $x = 0.0$, 0.3, and 0.5) to $CoAl_2O_4$. The obtained powders were labeled as $CoAl_2O_4$, $Mn_{0.3}Co_{0.7}Al_2O_4$ and $Mn_{0.5}Co_{0.5}Al_2O_4$, respectively, and then used for further characterizations.

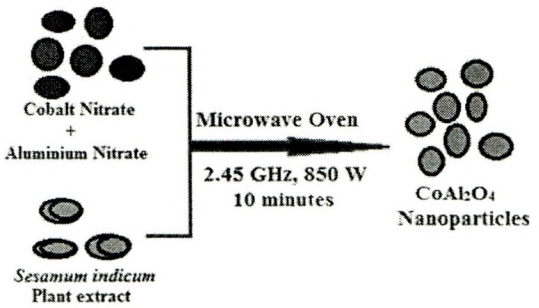

Scheme 1. Preparation procedure of spinel $CoAl_2O_4$ nanoparticles by *Sesamum indicum* plant extracted microwave-assisted combustion method.

2.2. Characterization Techniques

The structural characterization of spinel $Mn_xCo_{1-x}Al_2O_4$ ($x = 0.0$, 0.3 and 0.5) samples were performed using a Rigaku Ultima X-ray diffractometer (XRD) for 2θ values ranging from 10 to 80° using Cu-Kα radiation ($\lambda = 1.5418$ Å). The surface functional groups were analyzed by Perkin Elmer FT-IR spectrometer. The surface morphology of the samples was achieved at desired magnification with a Joel JSM 6360 high resolution scanning electron microscope (HR-SEM) equipped with energy dispersive X-ray (EDX) for elemental composition analysis. The transmission electron micrographs were carried out by Philips-TEM (CM20). The UV-Visible diffuse reflectance spectrum (DRS) was recorded using Cary100 UV-Visible spectrophotometer to estimate their band gap. The photoluminescence (PL) properties were recorded using Varian Cary Eclipse Fluorescence Spectrophotometer. Magnetic measurements were carried out at room temperature using a PMC MicroMag 3900 model vibrating sample magnetometer (VSM) equipped with 1 Tesla magnet.

2.3. Catalytic Test

The oxidation of benzyl alcohol using spinel $Mn_xCo_{1-x}Al_2O_4$ ($x = 0.0$, 0.3 and 0.5) samples was carried out in a batch reactor operated under atmospheric conditions. 5 mmol of oxidant (H_2O_2) was added along with 0.5 g of spinel $Mn_xCo_{1-x}Al_2O_4$ catalysts ($x = 0.0$, 0.3 and 0.5) and the contents were heated at 80 °C in an acetonitrile medium for 5 h in a three necked round bottom flask equipped with a reflux condenser and thermometer. The oxidized products after the catalytic reaction are collected and studied using Agilent GC spectrometer. The column used for the study was DB wax column (capillary column) of length 30 mm and helium was used as the carrier gas. GC technique was carried out to know the conversion percentage of the products. The yields of the benzaldehyde formed were calculated by the following formula (1) and (2),[30]

$$\text{Conversion (\%)} = \frac{\text{Std. peak area-Sample peak area}}{\text{Sample peak area}} \times 100 \quad (1)$$

$$\text{Selectivity (\%)} = \frac{\text{Sample peak area}}{\text{Total peak area}} \times 100 \quad (2)$$

3. RESULTS AND DISCUSSION

3.1. Powder X-ray Diffraction (XRD)

The crystal structure and phase purity of the powders were confirmed by analyzing the powder XRD patterns. Figures 1(a)–(c) shows the XRD patterns of spinel $Mn_xCo_{1-x}Al_2O_4$ ($x = 0.0$, 0.3 and 0.5) nanoparticles, respectively. The characteristic peaks at 2θ of 31.16, 36.86, 38.69, 44.57, 49.15, 55.79, 59.48, 65.59, 74.28 and 77.56° are corresponding to (220), (311), (222), (400), (331), (422), (511), (440), (620) and (533) diffraction planes. According to the XRD patterns, all diffraction peaks can be perfectly indexed as face centered cubic spinel $CoAl_2O_4$ (JCPDS card no. 38-0814).[31] The intensities and position of the peaks of the synthesized powders are in agreement with those of standard JCPDS and no other peak of any secondary phase was detected, which indicates that the prepared samples were pure crystalline materials.

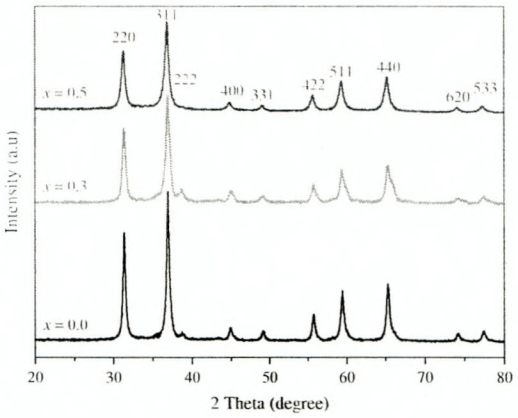

Figure 1. Powder XRD patterns of spinel $Mn_xCo_{1-x}Al_2O_4$ ($x = 0.0$, 0.3 and 0.5) samples.

The average crystallite size calculated from the most intense X-ray diffraction peak (311) using scherrer's Eq. (3),

$$D = \frac{0.89\lambda}{\beta \cos\theta} \quad (3)$$

where 'D' is the average crystallite size, 'λ', the X-ray wavelength, 'θ,' the Bragg diffraction angle and 'β', the full width at half maximum (FWHM). The average crystallite size was estimated by applying the Scherrer's equation on the peak at $2\theta = 36.86°$ for all samples and are shown in Table I. It was found that the average crystallite size was higher (20.65 nm) for pure $CoAl_2O_4$ while the crystallite size decreased from 18.76 nm to 16.14 nm for Mn-doped $CoAl_2O_4$ ($x = 0.3$ to 0.5). It can be seen that the widths of XRD peaks for the samples obtained at higher concentration of Mn-dopant ($Mn_{0.5}Co_{0.5}Al_2O_4$) are broader, indicating that the crystallite size is very smaller than other samples. The result reveals at Mn doping on $CoAl_2O_4$ sample controls and retards the growth of the crystallite size.

Table I. Crystallite size, BET surface area and band gap values of spinel $Mn_xCo_{1-x}Al_2O_4$ ($x = 0.0$, 0.3 and 0.5) nanoparticles.

Samples	Crystallite size (nm)	Band gap (eV)	BET surface area (m^2/g)
$CoAl_2O_4$	20.65	3.32	67.43
$Mn_{0.3}Co_{0.7}Al_2O_4$	18.76	3.46	70.26
$Mn_{0.5}Co_{0.5}Al_2O_4$	16.14	3.63	73.54

3.2. Fourier Transform Infrared (FT-IR) Analysis

Figures 2(a)–(c) show the FT-IR spectra of spinel $Mn_xCo_{1-x}Al_2O_4$ (x = 0.0, 0.3 and 0.5) nanoparticles. A broad absorption band centered in the region 3100–3500 cm^{-1}, which can be assigned to the vibrations of water H_2O molecules. The absorption band at 2357 cm^{-1} is due to the stretching vibration of CO_2. A band at around 1630 cm^{-1} is present in all compositions, which can be assigned to the H–O–H bending vibration. The bands at 827 cm^{-1}, 667 cm^{-1} and 560 cm^{-1} confirm the spinel structure of $CoAl_2O_4$. In all compositions of $CoAl_2O_4$ samples, the metal-oxygen stretching frequencies are reported in the range 500–900 cm^{-1}, associated with the vibrations of M–O, Al–O and M–O–Al bonds (M=Mn, Co).[32, 33] The results are in good agreement with the results obtained from the XRD analysis.

3.3. Scanning Electron Microscopy (SEM) Studies

The morphologies of spinel $Mn_xCo_{1-x}Al_2O_4$ (x = 0.0, 0.3 and 0.5) samples were confirmed by high resolution scanning electron microscope (HR-SEM) analysis. Figures 3(a)–(c) shows HR-SEM images of $CoAl_2O_4$, $Mn_{0.3}Co_{0.7}Al_2O_4$ and $Mn_{0.5}Co_{0.5}Al_2O_4$, respectively. HR-SEM images consist of agglomerated particle-like nanocrystals with uniform grain size smaller than 50 nm. It is believed that, during the combustion reaction, the microwave energy is used to nucleation growth of metallic Co^{2+} and Al^{3+} cations mixture obtained with a very short time was subjected in the microwave irradiation treatment to formed final products within few minutes of time with narrow size range was obtained.[23] The results proved that MACM route is a fast and easy method, due to the microwave energy can directly interact with the material interior, which results in a well-developed nano-sized particles and there is no need for further calcinations.

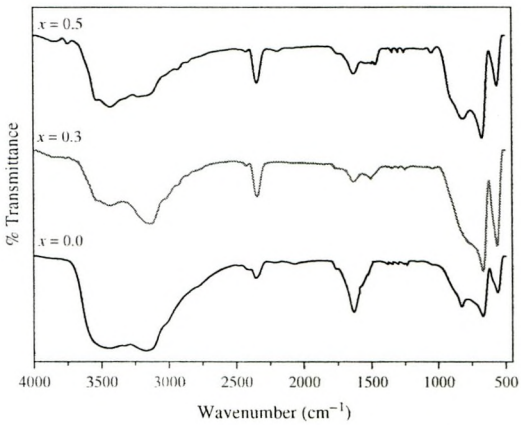

Figure 2. FT-IR spectra of spinel $Mn_xCo_{1-x}Al_2O_4$ (x = 0.0, 0.3 and 0.5) samples.

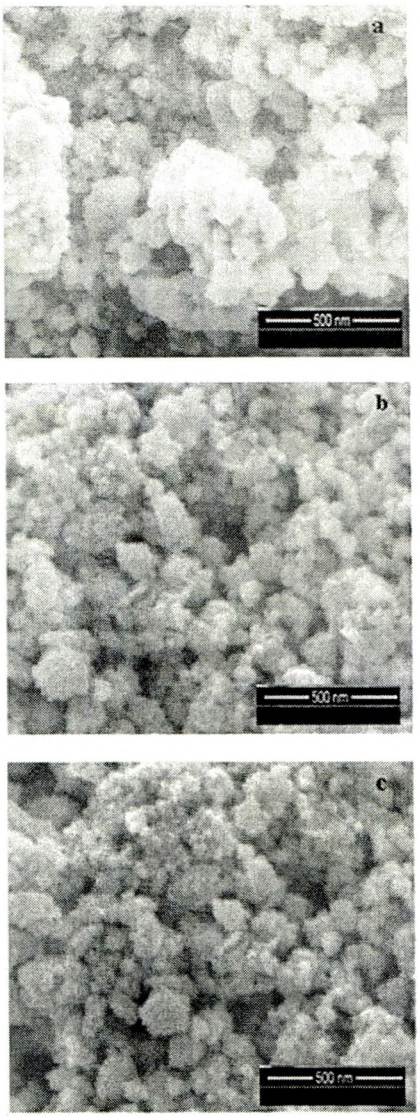

Figure 3. HR-SEM images of (a) $CoAl_2O_4$, (b) $Mn_{0.3}Co_{0.7}Al_2O_4$ and (c) $Mn_{0.5}Co_{0.5}Al_2O_4$ samples.

3.4. Transmission Electron Microscopy (TEM) Studies

The crystal structure, morphology and particle size of the samples were confirmed by high resolution transmission electron microscope (HR-TEM) analysis. Figure 4(a) show the HR-TEM images of $Mn_{.5}Co_{0.5}Al_2O_4$ sample. It was confirmed that the samples consists of particle-like nanocrystals with small amount of agglomerations. However, these nanoparticles are in the range of 15–22 nm in diameter; these values are in good agreement with the values obtained from XRD data. The selected area electron diffraction (SAED) pattern of the sample $Mn_{.5}Co_{0.5}Al_2O_4$,

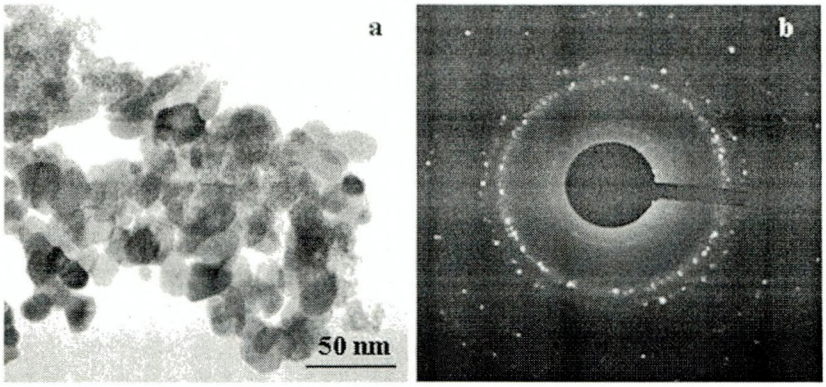

Figure 4. HR-TEM images (a) and SAED patterns (b) of $Mn_{0.5}Co_{0.5}Al_2O_4$ samples.

presented in the Figure 4(b), correspond to that of a spinel phase confirmation. The SAED pattern implies that the as-prepared spinel $CoAl_2O_4$ nano-crystals are good crystalline materials and single crystalline in nature.

The formation mechanism of spinel $Mn_xCo_{1-x}Al_2O_4$ ($x = 0.0$, 0.3 and 0.5) was proposed and the MACM route is one of the simplest methods for preparing of various functional nanomaterials. In this present study, MACM route was used successfully for synthesizing of $Mn_xCo_{1-x}Al_2O_4$ ($x = 0.0$, 0.3 and 0.5) nanoparticles using metal nitrates and *Sesamum indicum* plant extract gelling solution as raw materials. In this MACM synthesis, *Sesamum indicum* plant extracted solution act as a complexing and reducing agent, which is homogeneously mixes with metal cations in atomic scale and the microwave energy is used to nucleation growth of metallic Co^{2+} and Al^{3+} cations mixture obtained with a very short time and formed final products within few minutes of time.[30]

3.5. Energy Dispersive X-ray (EDX) Studies

Elemental composition of the samples was confirmed by Energy dispersive X-ray (EDX) analysis. Figures 5(a), (b) shows the EDX spectra of $CoAl_2O_4$ and $Mn_{0.5}Co_{0.5}Al_2O_4$, respectively. EDX results showed that the peaks of Mn, Co, Al and O elements in spinel $CoAl_2O_4$ and $Mn_{0.5}Co_{0.5}Al_2O_4$ samples, respectively and there is no other peak, which confirmed the as-prepared samples are pure products. The percentage of Co/Mn values obtained is given in inset of Figures 5(a), (b). Pure and Mn^{2+}-doped $CoAl_2O_4$ did not deviate from their initial stoichiometry and matched well with the initial degree of substitution. It is fascinating to note that the synthesis route entirely favors the formation of mixed spinel and allowing us to study the effect of increasing Mn^{2+} content on the properties of the $CoAl_2O_4$. However, a small peak is appeared at 2.1 KeV for both samples, which indicated the presence of gold (Au) peak and it is has been used as a sputter (gold) coating, while preparing the sample for HR-SEM recording for the better visibility of the surface morphology.

3.6. N_2 Adsorption/Desorption Isotherms

Surface area and the adsorbance competence of $Mn_xCo_{1-x}Al_2O_4$ nano-catalysts, BET surface area analysis was carried out. BET surface area studies revealed the

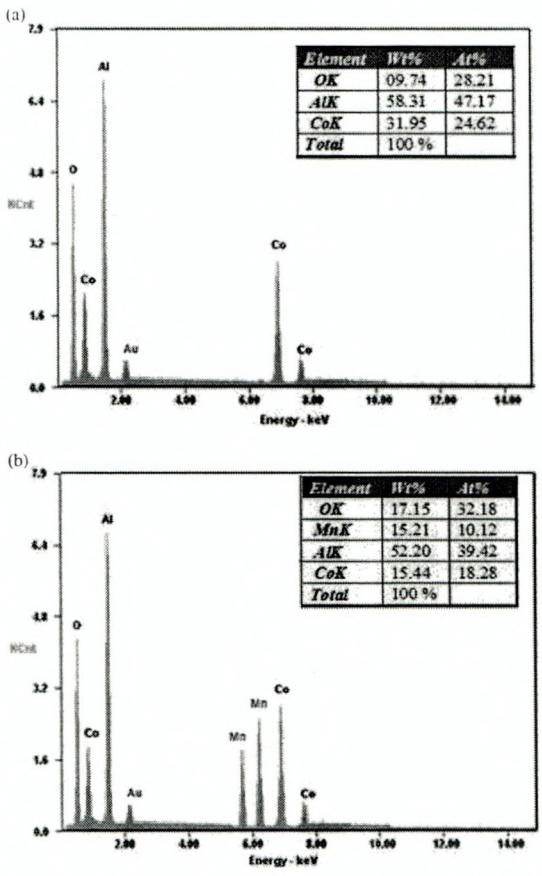

Figure 5. EDX spectra of of (a) $CoAl_2O_4$ and (b) $Mn_{0.5}Co_{0.5}Al_2O_4$ samples.

specific relation between the concentration of the adsorbate and its adsorption degree onto the adsorbent surface of the samples. It is well known that the surface area parameters of the samples varied according to the concentration of Mn^{2+} dopant on $Mn_xCo_{1-x}Al_2O_4$ nano-catalysts (Table I). However, the sample $Mn_{0.5}Co_{0.5}Al_2O_4$ has higher surface area (73.54 m^2/g) than other samples. In MACM synthesis route, an efficient and a homogeneous heating would result in a rapid and uniformity nucleation followed by the growth of spinel $Mn_xCo_{1-x}Al_2O_4$ nanoparticles.

3.7. Diffuse Reflectance Spectroscopy (DRS)

The fundamental process of UV-Visible absorption/reflectance/transmittance of light by nano-sized semiconducting metal oxides is significant to their electronic structures. Hence, the UV-Visible diffuse reflectance spectroscopy (DRS) study plays a vital role in estimating the band gap energy of the materials. The optical energy band gap was calculated using Tauc relation.[34] The Kubelka-Munk function is generally applied to convert the diffuse reflectance into equivalent absorption coefficient and mostly used for analyzing the powder samples.[35] The Kubelka-Munk function $F(R)$ was used to calculate the band gap energy of spinel $Mn_xCo_{1-x}Al_2O_4$ samples. Thus the vertical axis is converted into quantity $F(R)$ which is equal to the absorption co-efficient. Thus the 'α' in the Tauc equation is substituted with $F(R)$ and hence the relation becomes,

$$(F(R)) = \alpha = \frac{(1-R)^2}{2R} \tag{4}$$

where, $F(R)$ is Kubelka-Munk function, 'α' the absorption coefficient, 'R' the reflectance. Thus the Tauc relation becomes,

$$F(R)hv = A(hv - E_g)^n \tag{5}$$

where $n = 1/2$ and 2 for direct and indirect transitions, respectively, thus giving direct and indirect band gaps. The plots of $(F(R)hv)^2$ versus hv for all compositions are shown in Figure 6. Extrapolation of linear regions of these plots to $(F(R)hv)^2 = 0$ gives the direct band gap values.

The optical band gap energy values for all composition of $Mn_xCo_{1-x}Al_2O_4$ as shown in Table I. The direct band gap value of the pure $CoAl_2O_4$ was observed to be 3.32 eV, and it is increased with increasing the concentration of Mn^{2+}-dopant. The observed higher band gap energy of undoped $CoAl_2O_4$ sample is due to larger particle size.[36] Conversely, the band gap energy increased from 3.46 eV to 3.63 eV with increase in Mn^{2+} content ($x = 0.3$ to 0.5) in $CoAl_2O_4$ matrix, due to decrease of particle size. The increase of band gap energy may also be due to the sp-d exchange interaction between the localized d-electrons of Mn^{2+} ions and band electrons of $CoAl_2O_4$. Thus, the contraction of band gap with Mn^{2-} doping could be due to the formation of sub-bands in between the energy band gap and merging of their sub-bands with the conduction band to form a continuous band.[37]

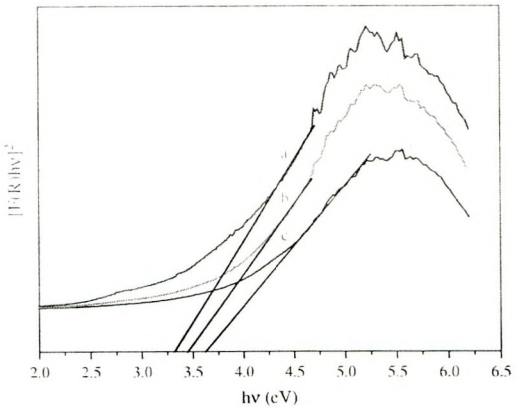

Figure 6. UV-Vis DRS spectra of (a) $CoAl_2O_4$, (b) $Mn_{0.3}Co_{0.7}Al_2O_4$ and (c) $Mn_{0.5}Co_{0.5}Al_2O_4$ samples.

3.8. Photoluminescence (PL) Studies

Photoluminescence (PL) spectra were recorded to investigate the recombination phenomena of semiconducting materials. Moreover, PL spectrum gives the information about the band gap with the relative active position of sub band gap and defect states of the semiconductors.[38, 39] Generally, $CoAl_2O_4$ is employed as the spinel type material, and doped with transition metals (e.g., Cu and Mn) as the activator and co-activator. However, in this present study, we have reported PL properties of spinel $CoAl_2O_4$ doped with Mn^{2+}. Figure 7 demonstrates the room temperature PL spectra recorded at $\lambda_{ex} = 310$ nm of $CoAl_2O_4$ samples prepared with various doping concentration of Mn^{2+} content. A small band is observed at 358 nm is ascribed to the near band-edge emission of wide band gap of $CoAl_2O_4$ due to the recombination of free excitons through an exciton-exciton process. In the present study, spinel $Mn_xCo_{1-x}Al_2O_4$ ($x = 0.0$, 0.3 and 0.5) samples

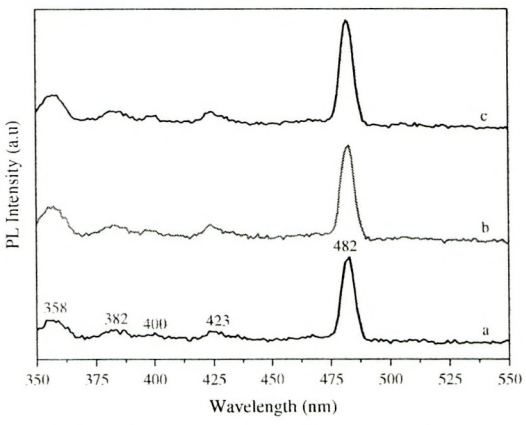

Figure 7. PL spectra of (a) $CoAl_2O_4$, (b) $Mn_{0.3}Co_{0.7}Al_2O_4$ and (c) $Mn_{0.5}Co_{0.5}Al_2O_4$ nanoparticles.

shows a peak corresponding to violet emission centered at 423 nm, due to the radiating defects related to the interface traps existing at the grain boundaries. Also, a blue emission (482 nm) appeared which represent a deep level visible emissions associated with localized levels in the band gap.[40] However, it is observed that doping of Mn^{2+} in $CoAl_2O_4$ lattice increased the luminescence intensity with an increase the Mn^{2+} dopant. Thus, the results are suggested that various emissions in spinel $Mn_xCo_{1-x}Al_2O_4$ arises, due to the defect centers that act as trap levels, which leads to the appearance of new electronic energy levels between the valence and the conduction band.[41]

3.9. VSM Measurements

The magnetic behavior of spinel $Mn_xCo_{1-x}Al_2O_4$ ($x = 0.0$, 0.3 and 0.5) nanoparticles were investigated by using the external magnetic field between ±15 kOe using room temperature vibrating sample magnetometer (VSM). Magnetizations (M) versus magnetic field (H) behavior plots are shown in Figure 8. The observed saturation magnetization (M_s), remanent magnetization (M_r) and coercivity (H_c) values are reported in Table II. These M–H curves are typical for a soft magnetic material and indicate superpara (pure $CoAl_2O_4$) and weak ferromagnetism (Mn^{2+}-doped $CoAl_2O_4$: $x = 0.3$ and 0.5), respectively, in the field ranges of ±15 kOe. Pure and Mn^{2+}-doped $CoAl_2O_4$ nanoparticles display 'hysteresis' type curve and the magnetization increased with increasing Mn^{2+} ions. The obtained result show that the value of M_s is lower (1.465×10^{-4} emu/g) for undoped $CoAl_2O_4$, and it is increased from 20.64×10^{-4} emu/g to 62.23×10^{-4} emu/g with increase the concentration of Mn^{2+} ($x = 0.3$ to 0.5), which can be attributed to the high magnetic nature of Mn^{2+} ions (5 μB) substituted by the lower magnetic moments of Co^{2+} (3 μB) ions in the spinel $CoAl_2O_4$ lattice.[42–44] However, it is observed that lower H_c and M_r values confirm that pure and Mn^{2+} in $CoAl_2O_4$ nanoparticles have

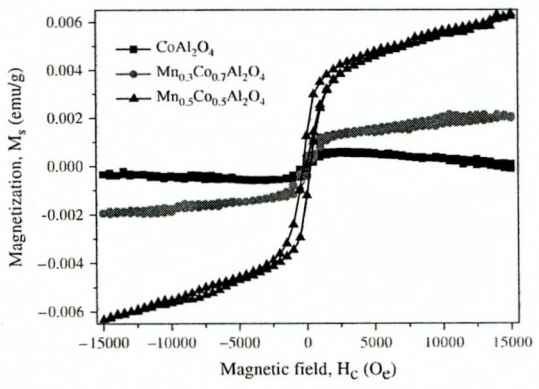

Figure 8. Magnetic hysteresis (M–H) loops of spinel $Mn_xCo_{1-x}Al_2O_4$ ($x = 0.0$, 0.3 and 0.5) nanoparticles.

Table II. Magnetic properties (magnetization, remanence and coercivity) of $Mn_xCo_{1-x}Al_2O_4$ ($x = 0.0$, 0.3 and 0.5) nanoparticles.

Samples	H_c (Oe)	M_r ($\times 10^{-4}$) (emu/g)	M_s ($\times 10^{-4}$) (emu/g)
$CoAl_2O_4$	252.99	2.213	1.465
$Mn_{0.3}Co_{0.7}Al_2O_4$	269.62	4.245	20.64
$Mn_{0.5}Co_{0.5}Al_2O_4$	277.54	12.41	62.23

soft nature of superpara and weak ferromagnetism respectively, due to the exchange between the ions occupying the tetrahedral and octahedral sites.[45–47]

3.10. Catalytic Tests

It is well known that the catalytic activity of nanomaterials depends strongly on particle size, morphology and structure. Nano-materials have been receiving increased attention, because they exhibit unusual properties that are significantly different from those of relatively larger particles of the same materials.[48–51] These unusual properties have been attributed to the extremely small sizes and the high specific surface area of the nano-catalysts. In the present study, the liquid phase catalytic oxidation of benzyl alcohol into benzaldehyde was carried out using the spinel $Mn_xCo_{1-x}Al_2O_4$ ($x = 0.0$, 0.3 and 0.5) nanocatalysts. Catalytic studies showed that the nature and concentration of dopant ions had a strong influence on both the conversion and product selectivity. The catalytic results were summarized in Table III.

Generally, the catalyst with a high specific surface area has a favorable effect on the catalytic activity. In this present work, the surface area of the $Mn_xCo_{1-x}Al_2O_4$ ($x = 0.0$, 0.3 and 0.5) nano-catalysts gradually increased with the increase of Mn^{2+} content ($x = 0.5$). However, the sample $Mn_{0.5}Co_{0.5}Al_2O_4$ had higher surface area (73.54 m^2/g) than other samples, due to the smaller size of $Mn_{0.5}Co_{0.5}Al_2O_4$ particles. Furthermore, the sample $Mn_{0.5}Co_{0.5}Al_2O_4$ showed better catalytic activity than other samples (Fig. 9). However, the higher specific surface area of $Mn_{0.5}Co_{0.5}Al_2O_4$ nano-particles was useful to catalytic activity via enhancing the adsorption of benzyl alcohol, which is the determining step in the catalytic reaction. It was found that the conversion of benzyl alcohol to benzaldehyde for the sample $Mn_{0.5}Co_{0.5}Al_2O_4$ was 92.43% with 100% selectivity, whereas for the pure $CoAl_2O_4$, the conversion was only 83.65% with 100% selectivity.

Table III. The conversion and selectivity percentage for the oxidation of benzyl alcohol into benzaldehyde (Reaction conditions: Catalyst ($Mn_xCo_{1-x}Al_2O_4$: $x = 0.0$, 0.3 and 0.5), 0.5 g; Benzyl alcohol, 5 mmol; Acetonitrile, 5 mmol; H_2O_2, 5 mmol; Temperature, 80 °C, time, 5 h).

Samples	Conversion (%)	Selectivity (%)
$CoAl_2O_4$	83.65	100
$Mn_{0.3}Co_{0.7}Al_2O_4$	89.26	100
$Mn_{0.5}Co_{0.5}Al_2O_4$	92.43	100

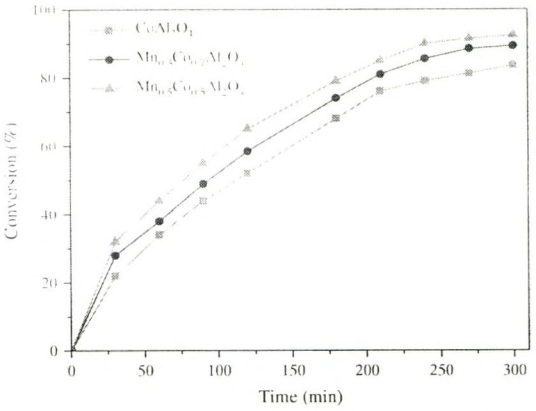

Figure 9. Catalytic activities (Reaction conditions: Catalyst ($Mn_xCo_{1-x}Al_2O_4$: $x = 0.0$, 0.3 and 0.5), 0.5 g; Benzyl alcohol, 5 mmol; Acetonitrile, 5 mmol; H_2O_2, 5 mmol; temperature, 80 °C, time, 5 h).

Besides, as the particle size decreases, the number of surface active sites increases in the catalysts. Thus, it is expected that the sample $Mn_{0.5}Co_{0.5}Al_2O_4$ nano-particles with very smaller particle size distribution would be a potentially efficient catalyst, due to the larger surface area coverage and better adsorption behavior, which in turn leads to the efficient catalysis.[52]

3.11. Reusability Studies

The catalytic oxidation of benzyl alcohol into benzaldehyde was employed as a model reaction to investigate the reusability of spinel $Mn_{0.5}Co_{0.5}Al_2O_4$ nano-catalyst. The recycling of the catalyst is very important for industrial and technological applications. The reusability of the catalyst for the liquid phase oxidation of benzyl alcohol into benzaldehyde was evaluated and the results are shown in Figure 10. For the reusability study purpose,

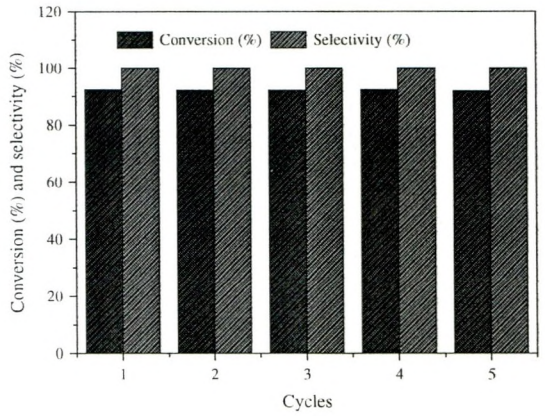

Figure 10. The reusability of the spinel $Mn_{0.5}Co_{0.5}Al_2O_4$ catalyst for the catalytic oxidation of benzyl alcohol to benzaldehyde.

the sample $Mn_{0.5}Co_{0.5}Al_2O_4$ nano-catalysts was filtered off from each run and washed several times with ethanol and dried at 110 °C in an air oven for 2 h and was checked for five consecutive runs under the identical conditions. During the five runs investigated, the conversion of benzyl alcohol was in a range from 92.32 to 92.28% for the sample $Mn_{0.5}Co_{0.5}Al_2O_4$, indicating that these catalyst displays good reproducibility and stability. Since, the spinel $Mn_{0.5}Co_{0.5}Al_2O_4$ nano-catalyst is able to oxidize benzyl alcohol into benzaldehyde with high activity, highly recyclable, remarkably stable and environmental friendly, they are promising candidates for the industrial applications.

4. CONCLUSIONS

Spinel $Mn_xCo_{1-x}Al_2O_4$ ($x = 0.0$, 0.3 and 0.5) nano-catalysts were successfully prepared by a simple MACM route using *Sesamum indicum (S. indicum)* plant extracted solution. Effects of Mn^{2+} doping on structural, morphological, opto-magnetic and catalytic properties were investigated. XRD, EDX and SAED results indicate that the as-synthesized samples have spinel structure without any other phase impurities. The appearance of broad band between 500 and 900 cm^{-1} in FT-IR spectra revealed the formation of M–O, Al–O and M–O–Al bonds in the spinel structure. HR-SEM and HR-TEM images depicted the formation of well developed particle-like morphology with nano-sized grains below 50 nm. UV-Visible DRS results showed the band gap value of pure $CoAl_2O_4$ is 3.32 eV and it was increased from 3.46 eV to 3.63 eV with increasing the Mn^{2+}-dopant ($x = 0.3$ to 0.5). VSM studies revealed that the pure and Mn^{2+} in $CoAl_2O_4$ showed superpara and ferromagnetism, respectively. It was found that $Mn_{0.5}Co_{0.5}Al_2O_4$ is highly active towards the selective oxidation of benzyl alcohol into benzaldehyde with the conversion of 92.43% with 100% selectivity. Moreover, this method of preparation is economically and environmentally friendly approach.

Acknowledgment: One of the authors, A. Manikandan is thankful to CSIR, New Delhi, India, for the award of Senior Research Fellowship (CSIR-SRF).

References and Notes

1. K. Ariga, T. Mori, and J. P. Hill, *Adv. Mater.* 24, 158 (**2012**).
2. M. A. Kamran, R. Liu, L. Jing, L. J. Shi, and B. Zou, *Nanosci. Nanotechnol. Lett.* 6, 706 (**2014**).
3. L. Wang, S. Tang, and H. Zhou, *Sci. Adv. Mater.* 5, 822 (**2013**).
4. Q. He, J. Liu, J. Liang, C. Huang, and W. Li, *Nanosci. Nanotechnol. Lett.* 6, 385 (**2014**).
5. P. Karipoth and R. J. Joseyphus, *Sci. Adv. Mater.* 6, 1792 (**2014**).
6. H. Liu, W. Li, H. Li, X. Zhang, L. Fei, Y. Liu, and J. Yang, *Nanosci Nanotechnol. Lett.* 6, 904 (**2014**).
7. S. Kumar, P. Sharma, and V. Sharma, *Sci. Adv. Mater.* 5, 713 (**2013**).
8. M. Y. Rafique, L. Pan, M. Z. Iqbal, Q. Javed, H. Qiu, M. H. Farooq, G. Zhengang, and M. A. Iqbal, *Nanosci. Nanotechnol. Lett.* 5, 791 (**2013**).

9. Y. Sun, Y. Guo, J. Li, C. Wang, X. Wang, C. I. Sathish, and K. Yamaura, *Sci. Adv. Mater.* 6, 1394 (**2014**).
10. J. Mohapatra, D. K. Mishra, S. K. Singh, B. Mahato, and A. Mitra, *Nanosci. Nanotechnol. Lett.* 5, 563 (**2013**).
11. D. V. Kurmude, C. M. Kale, P. S. Aghav, D. R. Shengule, and K. M. Jadhav, *J. Supercond. Nov. Magn.* 27, 1889 (**2014**).
12. Y. Koseoglu, *Ceram. Int.* 39, 4221 (**2013**).
13. M. Davis, C. Gunneci, R. Alsup, C. Korzeniewski, and L. J. H. Weeks, *Mater. Lett.* 73, 139 (**2012**).
14. M. Kumar, T. K. Seshagiri, M. Mohapatra, V. Natarajan, and S. V. Godbole, *J. Lumin.* 132, 2810 (**2012**).
15. R. Pandey, J. D. Gale, S. K. Sampath, and J. M. Recio, *J. Am. Ceram. Soc.* 82, 3337 (**1999**).
16. J. Song, M. Leng, X. Fu, and J. Liu, *J. Alloys Compd.* 543, 142 (**2012**).
17. M. Zawadzki, *Solid State Sci.* 8, 14 (**2006**).
18. F. Davar and M. S. Niasari, *J. Alloys Compd.* 509, 2487 (**2011**).
19. S. Kurajica, J. Popovic, E. Tkalcec, B. Grzeta, and V. Mandic, *Mater. Chem. Phys.* 135, 587 (**2012**).
20. M. Zayat and D. Levy, *Chem. Mater.* 12, 2763 (**2000**).
21. F. L. Yu, Y. Ma, J. Y. Du, and J. Zhou, *J. Alloys Compd.* 468, 443 (**2009**).
22. W. D. Li, J. Z. Li, and J. K. Guo, *J. Eur. Ceram. Soc.* 23, 2289 (**2003**).
23. S. M. Rafiaei, A. Kim, and M. Shokouhimehr, *Nanosci. Nanotechnol. Lett.* 6, 692 (**2014**).
24. I. E. Suliman, H. Eftekhari, S. M. Mohseni, and M. M. Tehranchi, *J. Supercond. Nov. Magn.* 24, 1263 (**2011**).
25. M. Jin, Z. Wang, H. Jiang, Y. Sun, X. Wang, H. Qian, Q. Chen, and K. Liu, *J. Supercond. Nov. Magn.* 26, 2779 (**2013**).
26. D. Visinescu, B. Jurca, A. Ianculescu, and O. Carp, *Polyhedron* 30, 2824 (**2011**).
27. V. G. Bairi, S. E. Bourdo, U. B. Nasini, S. K. Ramasahayam, F. Watanabe, B. C. Berry, and T. Viswanathan, *Sci. Adv. Mater.* 5, 1275 (**2013**).
28. C. H. Huang, S. J. Liu, S. F. Lee, W. S. Hwang, and C. F. Lin, *Sci. Adv. Mater.* 5, 1737 (**2013**).
29. E. Shirmohammadi, G. R. Bagheri, S. Saeidi, T. Mohasseli, Z. Mohkami, G. S. Baigi, T. Naruei, and F. Javadian, *Eur. J. Experimen. Biology*, 4, 197 (**2014**).
30. A. Manikandan, R. Sridhar, S. A. Antony, and S. Ramakrishna, *J. Mol. Struct.* 1076, 188 (**2014**).
31. W. Walerczyk, M. Zawadzki, and H. Grabowska, *Catal. Lett.* 141, 592 (**2011**).
32. G. A. Sigel, R. A. Bartlett, D. Decker, M. M. Olmstead, and P. P. Power, *Inorg. Chem.* 26, 1773 (**1987**).
33. J. P. Ramirez, G. Mul, F. Kapteijn, and J. A. Moulijn, *J. Mater. Chem.* 11, 821 (**2001**).
34. S. F. Wang, F. Gu, M. K. Lu, X. F. Cheng, W. G. Zou, G. J. Zhou, S. M. Wang, and Y. Y. Zhou, *J. Alloys Compd.* 394, 255 (2005).
35. H. Bai, Z. Liu, and D. D. Sun, *Int. J. Hydrogen Energy* 37, 13998 (**2012**).
36. E. M. A. Jamal, D. S. Kumar, and M. R. Anantharaman, *Bull. Mater. Sci.* 34, 251 (**2011**).
37. A. S. Ahmed, S. M. Muhamed, M. L. Singk, S. Tabassum, A. H. Naqvi, and A. Azam, *J. Lumin.* 131, 1 (**2011**).
38. T. Schmidt, K. Lischka, and W. Zulehner, *Phys. Rev. B* 45, 8989 (**1992**).
39. R. K. Sendi and S. Mahmudm, *Appl. Surf. Sci.* 258, 8026 (**2012**).
40. R. Bhargava, P. K. Sharma, R. K. Dutta, S. Kumar, A. C. Pandey, and N. Kumar, *Mater. Chem. Phys.* 120, 393 (**2010**).
41. Y. Shen, W. Li, and T. Li, *Mater. Lett.* 65, 2956 (**2011**).
42. N. S. Ferreira, L. G. Abracado, and M. A. Macedo, *J. Supercond. Nov. Magn.* 26, 2549 (**2013**).
43. L. Xu, H. Zhang, K. Shen, M. Xu, and Q. Xu, *J. Supercond. Nov. Magn.* 25, 1951 (**2012**).
44. A. Manikandan and S. A. Antony, *J. Supercond. Nov. Magn.* (**2014**), DOI 10.1007/s10948-014-2634-9.
45. Y. Ichiyanagi, Y. Kimishima, and S. Yamada, *J. Magn. Magn. Mater.* 272, E1245 (**2004**).
46. A. S. Bhatt, D. K. Bhat, C. Tai, and M. S. Santosh, *Mater. Chem. Phys.* 125, 347 (**2011**).
47. S. Daengsakul, C. Thomas, C. Mongkolkachit, and S. Maensiri, *Sci. Adv. Mater.* 5, 242 (**2013**).
48. E. Karaoglu and A. Baykal, *J. Supercond. Nov. Magn.* 27, 2041 (**2014**).
49. J. Mohapatra, D. K. Mishra, S. K. Singh, B. Mahato, and A. Mitra, *Nanosci. Nanotechnol. Lett.* 5, 563 (**2013**).
50. L. S. Silva, S. Gil, N. Gutierrez, A. Romero, and J. L. Valverde, *Sci. Adv. Mater.* 5, 1907 (**2013**).
51. S. K. Mehta and S. Gupta, *Sci. Adv. Mater.* 5, 1377 (**2013**).
52. A. Baykal, E. Karaoglu, H. Sozeri, E. Uysal, and M. S. Toprak, *J. Supercond. Nov. Magn.* 26, 165 (**2013**).

Received: 9 September 2014. Accepted: 5 October 2014.